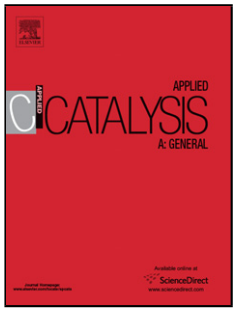

Title: Selective oxidation of propylene to acrolein by hydrothermally synthesized bismuth molybdates

Author: Kirsten Schuh Wolfgang Kleist Martin Høj Vanessa Trouillet Pablo Beato Anker Degn Jensen Greta R. Patzke Jan-Dierk Grunwaldt

PII: S0926-860X(14)00372-X
DOI: http://dx.doi.org/doi:10.1016/j.apcata.2014.05.038
Reference: APCATA 14858

To appear in: *Applied Catalysis A: General*

Received date: 1-3-2014
Revised date: 22-5-2014
Accepted date: 27-5-2014

Please cite this article as: K. Schuh, W. Kleist, M. Hoj, V. Trouillet, P. Beato, A.D. Jensen, G.R. Patzke, J.-D. Grunwaldt, Selective oxidation of propylene to acrolein by hydrothermally synthesized bismuth molybdates, *Applied Catalysis A, General* (2014), http://dx.doi.org/10.1016/j.apcata.2014.05.038

Selective oxidation of propylene to acrolein by hydrothermally synthesized bismuth molybdates

Kirsten Schuh, Wolfgang Kleist, Martin Høj, Vanessa Trouillet, Pablo Beato, Anker Degn Jensen, Greta R. Patzke and Jan-Dierk Grunwaldt*

Kirsten Schuh, Dr. Wolfgang Kleist, Prof. Dr. Jan-Dierk Grunwaldt
Karlsruhe Institute of Technology (KIT), Institute for Chemical Technology and Polymer Chemistry (ITCP) and Institute of Catalysis Research and Technology (IKFT), Engesserstr. 20, 76131 Karlsruhe (Germany)

Dr. Martin Høj, Prof. Dr. Anker Degn Jensen
Technical University of Denmark (DTU), Department of Chemical & Biochemical Engineering, Søltofts Plads, 2800 Kgs. Lyngby (Denmark)

Prof. Dr. Greta R. Patzke
University of Zurich (UZH), Institute of Inorganic Chemistry, Winterthurerstrasse 190, CH-8057 Zurich (Switzerland)

Vanessa Trouillet
Karlsruhe Institute of Technology (KIT), Institute for Applied Materials (IAM) and Karlsruhe Nano Micro Facility (KNMF), Hermann-von-Helmholtz-Platz 1, 76344 Eggenstein-Leopoldshafen (Germany)

Dr. Pablo Beato
Haldor Topsøe A/S, Nymøllevej 55, 2800 Kgs. Lyngby (Denmark)

KEYWORDS: Bismuth molybdates; hydrothermal synthesis; unsupported catalysts; selective propylene oxidation; acrolein

ABSTRACT: Hydrothermal synthesis has been used as a soft chemical method to prepare bismuth molybdate catalysts for the selective oxidation of propylene to acrolein. All obtained samples displayed a plate-like morphology, but their individual aspect ratios varied with the hydrothermal synthesis conditions. Application of a high Bi/Mo ratio during hydrothermal synthesis afforded γ-Bi_2MoO_6 as the main phase, whereas lower initial bismuth contents promoted the formation of α-$Bi_2Mo_3O_{12}$. Synthesis with a Bi/Mo ratio of 1:1 led to a phase mixture of α- and γ-bismuth molybdate showing high catalytic activity. The use of nitric acid during hydrothermal synthesis enhanced both propylene conversion and acrolein yield, possibly due to a change in morphology. Formation of β-$Bi_2Mo_2O_9$ was not observed under the applied conditions. In general, the catalytic performance of all samples decreased notably after calcination at 550 °C due to sintering.

1. Introduction

The typical commercial catalyst for the selective oxidation of propylene to acrolein and for propylene ammoxidation to acrylonitrile is based on bismuth molybdates as the active species in combination with additional elements such as Co, Ni, Fe, Cr, Al or alkali metals [1, 2]. Transition metal molybdates, especially $CoMoO_4$ or $Fe_2(MoO_4)_3$ and their solid solutions, increase the ability to exchange electrons and oxygen anions due to the effective activation of molecular oxygen by Co^{2+} and Fe^{3+}. They change the morphology of the catalyst under the reaction conditions along with recently reported synergistic effects of the different phases [3-5]. Other elements, including alkali metals, W, V, Nb etc. are usually added to enhance the catalyst life time and its mechanical strength. They also lead to minor improvements in activity and selectivity [6, 7].

Various bismuth molybdates including α-$Bi_2Mo_3O_{12}$, β-$Bi_2Mo_2O_9$ and γ-Bi_2MoO_6 have been prepared and tested as oxidation catalysts [8]. Whereas γ-Bi_2MoO_6 exhibits an Aurivillius-type structure with alternating $[Bi_2O_2]^{2+}$ slabs and layers of corner sharing MoO_6 octahedra, both the α- and the β-phase can be considered as defective fluorite structures consisting of tetrahedral MoO_4 motifs. At temperatures above 570 °C the metastable γ''-phase is formed which is further transferred to the high-temperature γ'-phase at 640 °C. γ´-Bi_2MoO_6, which is also known as the γ(H)-phase, also has a fluorite like structure based on MoO_4 tetrahedra [9]. The metastable phase β-$Bi_2Mo_2O_9$ can usually be accessed in the temperature range from 540 to 665 °C [10].

Despite extensive preceding studies, there is an ongoing debate in literature about the relative catalytic activity of these phases [11, 12]. The group of Keulks [4, 11] found the γ-Bi_2MoO_6 phase to be most active, whereas Burrington and Grasselli [13] stated that the β-phase showed the highest rates for propylene oxidation. Carson et al. [14] prepared the different bismuth molybdate phases by co-precipitation at pH = 7 and found that the catalytic activity for propylene oxidation decreased in the following order: α > γ > β. They further concluded that a mechanical mixture of α-$Bi_2Mo_3O_{12}$ and γ-Bi_2MoO_6 was more active and selective in propylene oxidation to acrolein than the according pure phases. This synergistic effect was confirmed by Bing et al. [12], who suggested that the γ-phase

generated the active oxygen species, while the α-phase contributed the selective sites for acrolein formation. According to Le et al. [15] the synergistic effect was only observed in mixtures containing the γ-phase in close contact to the other phases.

The most common method to prepare bismuth molybdate catalysts is co-precipitation [16, 17] followed by calcination or solid-state reaction [18] at temperatures up to 1000 °C, but also sol-gel synthesis [19] or spray drying [20] were applied. These synthesis routes require harsh conditions and high temperatures to obtain crystalline products, which may influence the catalytic activity of the resulting phase. van Well et al. [21] found that the activity of γ-Bi_2MoO_6 prepared by co-precipitation and spray drying strongly depended on the calcination conditions. Alternatively γ-Bi_2MoO_6 has been synthesized under hydrothermal conditions applying cetyltrimethylammonium bromide (CTAB) as a surfactant [22] or using sodium, chlorine or fluorine containing reactants [23, 24], which may remain in the product and influence its catalytic performance. Hydrothermal processes are typical soft chemistry ('chimie douce') approaches which provide convenient access to advanced materials of high crystallinity, high purity, narrow size distribution and a low degree of aggregation [8]. Beale and Sankar [25] prepared α- and γ-bismuth molybdate in a one step hydrothermal synthesis from Bi_2O_3 dissolved in nitric acid and ammonium molybdate dissolved in ammonium hydroxide. Synthesis with β-phase stoichiometry (Bi/Mo = 2:2) and variation of the pH value did not yield β-$Bi_2Mo_2O_9$ under hydrothermal conditions so that heat treatment was required [8].

In the present study, mild hydrothermal techniques were applied to produce various bismuth molybdate phases with different morphologies and corresponding phase mixtures. The influence of calcination on the phase composition and the catalytic activity for propylene oxidation to acrolein has been studied in detail. However, to the best of our knowledge hydrothermally synthesized bismuth molybdates have not yet been applied for the selective oxidation of propylene to acrolein. In the following, we compare the properties of catalysts emerging from this flexible synthetic route to samples synthesized by conventional co-precipitation.

2. Experimental section

2.1. Synthesis.

The bismuth molybdate materials were synthesized by hydrothermal synthesis, while reference samples were obtained from conventional co-precipitation. All chemicals were analytical grade and used without further purification.

In a typical hydrothermal synthesis 10 mmol $Bi(NO_3)_3 \cdot 5H_2O$ and the stoichiometric amount of $(NH_4)_6Mo_7O_{24} \cdot 4H_2O$ (Bi/Mo ratios in the range of 0.5 – 3) were dissolved in 100 ml deionized water. These samples will be referred to here as HT_BixMoy with x/y being the Bi/Mo-molar ratio. Additionally for a ratio of Bi/Mo = 1:1 the pH was adjusted from 0.9 to 4 by addition of ammonium nitrate solution (HT_Bi1Mo1_pH4). 5 ml of nitric acid was added to the solution containing a Bi/Mo ratio of 1:1 and 2:1 referred to as HT_BixMoy_HNO3. Precursors with a Bi/Mo = 2:1 ratio were moreover dissolved in 80 ml of 25 vol.% acetic acid to lower the pH value from 0.8 to 0.2 (HT_Bi2Mo1_HOAc). The resulting solutions were heated in sealed 250 ml autoclaves (Berghof) with Teflon inlays at 180 °C for 24 h in an oven. After cooling to room temperature, the solid product was separated by filtration, washed with water, ethanol and finally with acetone. The resulting powder was dried at room temperature and ambient pressure. The samples prepared with a Bi/Mo ratio in the range 0.5 – 2 in water were also calcined at 550 °C for 4 h.

The corresponding co-precipitated samples were synthesized according to Carrazán et al.[6] using $(NH_4)_6Mo_7O_{24} \cdot 4H_2O$ dissolved in NH_4OH and $Bi(NO_3)_3 \cdot 5H_2O$ dissolved in HNO_3 at pH = 7. The resulting solid material was calcined at 450 °C to yield the α- and the γ-phases and at 680 °C to obtain the β-phase. Experiments are referred to as CP_BixMoy_CT where CT is the calcination temperature in °C.

2.2.Characterizatio**n.**

Powder X-ray diffraction (PXRD) measurements were recorded using a Bruker D8 Advance powder diffractometer in the range 2θ = 8 - 80° (step size 0.016 °) with Cu K_α radiation (Ni-filter, 45 mA, 35

kV) on rotating sample holders. Raman spectra were recorded with a Horiba Jobin Yvon spectrometer (LabRam) attached to an Olympus microscope (BX 40) using a 632.8 nm laser in the range 100 - 1100 cm^{-1} on an object slide without pretreatment of the sample.

The specific surface area (SSA) was measured by nitrogen adsorption at its boiling point (Belsorp II mini, BEL Japan Inc.) using multipoint BET theory in the $p/p_0 = 0.05 – 0.3$ range.

For scanning electron microscopy (SEM), performed on a Quanta 200 ESEM (FEG) microscope at the Centre of Electron Nanoscopy (CEN) at DTU, samples were deposited on a carbon foil on aluminium stubs and coated with carbon to improve the conductivity.

Surface analysis by X-ray photoelectron spectroscopy (XPS) was performed with a K-Alpha spectrometer (ThermoFisher Scientific) using a microfocused Al K_α X-ray source (400 µm spot size). Data acquisition and processing using Thermo Avantage software is described elsewhere. [26] Charge compensation during analysis was achieved using electrons of 8 eV energy and low energy argon ions to prevent any localized charge build-up. Spectra were fitted with one or more Voigt profiles (binding energy uncertainty: ±0.2 eV). [27, 28] Scofield sensitivity factors were applied for quantification. [29] The energy scale was calibrated to the binding energy of C 1s (C-C, C-H) at 285.0 eV controlled by means of the well known photoelectron peaks of metallic Cu, Ag and Au, respectively.

The bulk composition of the catalysts was determined by optical emission spectrometry with inductively coupled plasma (ICP-OES, Agilent 720/725-ES). The plasma was created by a 40 MHz high-frequency generator and argon was applied as the plasma gas. For the ICP-OES each sample was dissolved in 6 ml concentrated HNO_3, 2 ml concentrated HCl and 0.5 ml H_2O_2 in a microwave (at 600 Watt for 45 minutes).

Quantitative nitrogen analysis was carried out using hot gas extraction method (LECO TC 600). The samples were heated in a graphite crucible under flowing helium and thermally decomposed. The amount of N_2 gas was determined by a heat conductivity detector. Each measurement was repeated twice and a standard deviation was calculated.

2.3. Catalytic test reaction**.**

Catalytic activities were measured in a continuous flow fixed bed reactor, a U-shaped quartz reactor with 4 mm inner diameter. The catalyst powders were crushed and sieved to 150 – 300 µm particles and 500 mg of sample was loaded in the reactor and stabilized with quartz wool. The quartz reactor was connected to a commercial test unit (ChimneyLab Europe) with calibrated mass flow controllers (Brooks) and placed in an oven (Watlow) [30]. A thermocouple was placed inside the reactor just touching the catalyst bed to measure the reaction temperature and a pressure transducer placed upstream of the reactor measured the actual reaction pressure. The catalysts were pre-oxidized in dry air at 550 °C for the calcined hydrothermally synthesized samples and at 300 °C for all other samples. Activity tests were performed using a gas composition of $C_3H_6/O_2/N_2$ = 5/25/70 and flows of 50, 80, 120 Nml/min. The gas analysis was performed with a dual channel GC–MS (Thermo Fischer) with a TCD detector for quantifying N_2, O_2, CO and CO_2 and a FID detector parallel to the MS for identifying and quantifying saturated and unsaturated light hydrocarbons and oxygenated byproducts. The measured concentrations were corrected for expansion of the gas due to combustion using the nitrogen signal as internal standard, before calculating the conversion of propylene and the selectivity for acrolein.

3. Results and Discussion

3.1. Samples synthesized in pure aqueous hydrothermal media.

3.1.1. Characterization of the as-prepared bismuth molybdates.

Five different samples were prepared under hydrothermal conditions in pure water with Bi/Mo ratios from 0.5 – 3, and their phase composition was analyzed by powder X-ray diffraction (PXRD) and Raman spectroscopy. Only two different bimetallic phases were present in the products summarized in Table 1: α-$Bi_2Mo_3O_{12}$ and γ-Bi_2MoO_6. Application of a high Bi/Mo ratio led to the formation of the

bismuth-rich phase, γ-Bi_2MoO_6. Decreasing initial bismuth contents led to increasing amounts of α-$Bi_2Mo_3O_{12}$ in the as prepared samples. The diffraction pattern of the sample prepared with a high excess of bismuth (Bi/Mo = 3:1) displays characteristic reflections at 2θ = 28.3, 23.7 and 46.9 ° which can be assigned to γ-Bi_2MoO_6 (PDF 21-102 [31]) [32] and cubic BiO_{2-x} (PDF 47-1057) [33]. The crystallinity of HT_Bi3Mo1 was lower than the crystallinity of the other four samples, as indicated by the broader reflections in the diffraction pattern (Figure 1). This goes hand in hand with a significantly higher surface area than observed for the other four samples (30 m^2/g compared to 6 - 8 m^2/g). The diffraction pattern of the sample synthesized with Bi/Mo = 2:1 (Figure 1a) indicates γ-Bi_2MoO_6 as the main phase and additionally the presence of α-$Bi_2Mo_3O_{12}$ (low intensity reflection at 27.9°) and $Bi_6O_6(OH)_3(NO_3)_3 \cdot 1.5H_2O$ (10.3° and 31.3°, PDF 53-1038) [34]. The corresponding Raman spectrum of this sample depicted in Figure 1b confirmed the presence of γ-Bi_2MoO_6 as the main phase in this sample. The observed Raman bands at 848, 808, 792, and 714 cm^{-1} were assigned to Mo-O stretching frequencies of the distorted MoO_6 octahedra of the Aurivillius layered structure [32, 35]. Additionally, bands at 352, 323, 294 and 282 cm^{-1} were found, which correspond well to those reported for γ-Bi_2MoO_6 in the literature [36]. The presence of α-$Bi_2Mo_3O_{12}$ was evident from the band at 901 cm^{-1}, and the vibration at 1031 cm^{-1} could be assigned to a nitrate containing phase. This nitrate containing phase also led to a broader band at 782 – 808 cm^{-1} [37]. Quantitative nitrogen analysis yielded 0.36 wt.% (± 0.02 wt.%) N in this sample, which agrees well with the presence of a nitrate phase.

The ICP-OES measurement of HT_Bi2Mo1 showed that the product contained bismuth and molybdenum in the ratio 2:1, which corresponds well to the applied ratio.

Whereas distinction of the three different phases may be difficult with PXRD methods due to their adjacent main reflections (α: 27.9 °, β: 27.8 °, γ: 28.3 °) and the formation of the β-phase is easily overlooked, Raman spectra were recorded for a more precise and complementary identification of these three different bismuth molybdate phases.

The sample prepared with Bi/Mo = 1:1 contained a mixture of γ-Bi_2MoO_6 and α-$Bi_2Mo_3O_{12}$ according to PXRD measurements, whereas the Raman spectrum only displayed the α-phase. While X-ray diffraction measurements provide information of quantitative phase composition of larger particles, Raman spectra often only show the strongest bands which may overlap with band of other phases. The Raman spectrum of α-$Bi_2Mo_3O_{12}$ exhibited six bands between 1000 – 800 cm^{-1} which can be attributed to the Mo-O stretching modes of different tetrahedral species, i.e. 955 cm^{-1} (a_3), 925 cm^{-1} (a_1), 906 cm^{-1} (a_2), 856 cm^{-1} (a_1), 840 cm^{-1} (a_2) and 816 cm^{-1} (a_3). All of these six bands were present in the spectra of HT_Bi1Mo1 as well as in the spectra of the samples synthesized with a Bi/Mo ratio below 1:1 (Figure 1b).

The X-ray diffraction pattern and the Raman spectrum of the sample with an initial Bi/Mo ratio 2:3 showed the characteristic features of α-$Bi_2Mo_3O_{12}$ and indicated in addition the presence of a bismuth-free molybdenum oxide side phase (reflection at 25.7 °, Raman shift: 993 cm^{-1}). Calculation of the Bi/Mo ratio from the values obtained from ICP-OES measurements yielded to 0.7 (± 10%) (Table 1), corresponding to the Bi/Mo ratio in the α-phase. This indicates that, additionally to α-$Bi_2Mo_3O_{12}$ and an ammonium-containing molybdenum oxide phase, another bismuth oxide phase should be present which could not be detected by PXRD or Raman spectroscopy. Generally, such small amounts of bismuth oxides are difficult to identify from diffraction patterns due to the overlap of some of their reflections with those of bismuth molybdates. van Well et al. [21] also claimed that excess bismuth in form of β-Bi_2O_3 or β-$Bi_2Mo_2O_9$ cannot be seen by X-ray diffraction when the samples were calcined at temperatures lower than 500 °C.

The Raman spectrum of the sample synthesized with a high excess of molybdenum (HT_Bi1Mo2) illustrates the presence of the main γ-phase together with a band at 973 cm^{-1} which corresponds well to $NH_3(MoO_3)_3$ in agreement with PXRD data (reflections at 19.4 and 25.7°).

SEM images of all samples showed a plate-like morphology (Figure 2) with variations in aspect ratio and size. Synthesis with a large excess of bismuth led to the smallest particle size (Figure 2a and b), resulting in a relatively high specific surface area (30 m^2/g). The particles of sample HT_Bi2Mo1 were

rectangular with a side length of 1 - 2.5 µm and a thickness of ca. 200 nm (Figure 2c). Synthesis with Bi/Mo = 1:1 led to smaller plates (500 nm) with rounded edges (Figure 2e and f). SEM images of HT_Bi2Mo3 (Figure 2g and h) revealed a mixture of plates with a side length around 1 µm and larger needles / rods. HT_Bi1Mo2 (Figure 2d) morphologically displays two types of particles as well: the plate-like α-$Bi_2Mo_3O_{12}$ (400 nm – 1 µm in size) and the wedge-like / rod-like ammonium molybdenum oxide phase visible at the bottom of the image.

3.1.2. Catalytic performance of the as prepared bismuth molybdates.

The catalytic activity measurements for propylene oxidation of the as prepared samples are depicted in Figure 3. At 320 °C propylene conversion for all five samples remained below 10%. The sample prepared with a high excess of bismuth (HT_Bi3Mo1) exhibited propylene conversion up to 7.3% but the selectivity for acrolein was very low and mainly CO_x was formed. HT_Bi2Mo3 and HT_Bi1Mo2 yielded similar propylene conversion (2.6 – 7.2%) but HT_Bi1Mo2, which additionally to α-$Bi_2Mo_3O_{12}$ also contained $NH_3(MoO_3)_3$, exhibited lower acrolein selectivity (36 - 56% compared to 60 – 63%). Additionally to acrolein also CO_2, CO and acetaldehyde were formed. The synthesized sample with Bi/Mo = 2:1 (HT_Bi2Mo1) showed the highest acrolein yield at all three flows (120, 80 and 50 Nml/min). The surface areas of the hydrothermally synthesized samples with Bi/Mo = 0.5 - 2 were very similar (6 – 8 m^2/g; see Table 1) and therefore calculating propylene conversion on the basis of the surface area inside the reactor did not change the relative activities of the measured samples. At 360 °C all samples showed very similar activities resulting in a propylene conversion between 10% and 22% depending on the flow and accordingly on the contact time. Besides acrolein (60 - 90%) only CO_x (mainly CO_2) and traces of acetaldehyde were formed. The sample prepared with a large excess of bismuth (HT_Bi3Mo1) converted less propylene than the other four samples at 360 °C and was almost inactive for propylene oxidation. This sample was also not selective for acrolein and mainly produced hexadiene and CO_x. This agrees well with previous literature reports on the formation of hexadiene in the presence of Bi_2O_3 [38, 39]. HT_Bi2Mo1 also contained a bismuth oxide phase but its concentration may be too low to influence the catalytic activity of the sample. The presence of γ-

Bi_2MoO_6 as main product goes hand in hand with a slightly higher selectivity at lower conversion compared to the samples synthesized with lower Bi/Mo ratio. At higher temperature (400 °C) the propylene conversion increased up to 32% and the difference between the measurement points for each sample at similar conditions also raised (Figure 3b). The sample prepared with Bi/Mo = 1:1 was slightly more active than HT_Bi2Mo1 and their catalytic activity deteriorated with decreasing Bi/Mo ratio. The selectivity for acrolein was never below 60% and remained relatively constant with increasing propylene conversion indicating that acrolein further reacted to CO_x only very slowly on these catalysts. At temperatures above 400 °C the bismuth molybdates deactivated probably due to a loss of surface area loss and morphological changes. An increase of the reaction temperature from 440 °C to 520 °C did not result in an increase in propylene conversion and acrolein yield.

Note that as for most transition metal oxide catalysts the initial phase probably changed during the catalytic activity measurements from 320 – 520 °C, so that the phases summarized in the second column of Table 1 ("as-prepared") are not those actually present in the reactor during propylene conversion. We thus investigated the phase composition after the catalytic process as well.

Figure 4 shows the powder diffraction pattern of the hydrothermally synthesized samples after catalytic tests at temperatures up to 520 °C. Comparisons of the diffraction pattern and also of the Raman spectra of fresh and used catalysts indicate that the main phase of the catalysts did not change during the application in selective oxidation of propylene. Post-catalytic HT_Bi3Mo1 consisted of γ-Bi_2MoO_6 and $Bi_8Mo_3O_{21}$, which is orthorhombic and presents a basic fluorite-type structure [40, 41]. The minor phases in samples HT_Bi2Mo1 and HT_Bi2Mo3 indicated by only one or two low intensity reflections disappeared, whereas for the sample synthesized with a high excess of molybdenum (HT_Bi1Mo2) the hexagonal $NH_3(MoO_3)_3$-phase was transformed into α-MoO_3. SEM images in Figure 5 revealed that the plate-like morphology of the samples could not be preserved during the application for selective oxidation of propylene at 320 – 520 °C. Only the sample synthesized with the Bi/Mo ratio 2:1 partly retained its plate-like morphology (Figure 5d). All samples exhibited similar morphologies after the catalytic tests, whereas their particle sizes decreased with

increasing bismuth content. Generally, thermal treatment led to particle agglomeration and a significant loss of surface area (< 1 m^2/g). Post-catalytic samples only contained α-$Bi_2Mo_3O_{12}$ and / or γ-Bi_2MoO_6, except for sample HT_Bi1Mo2, where an excess of Mo led to the additional formation of α-MoO_3.

3.2. Influence of the calcination procedure on catalyst properties and activity

3.2.1. Characterization of calcined samples.

Hydrothermally synthesized samples with Bi/Mo ratios 0.5 – 2.0 (pure water) were calcined at 550 °C for 4 h to increase the phase purity of the products and to evaluate the transformation of the phases at elevated temperatures. Figure 6a depicts the PXRD patterns of the four calcined samples, and the corresponding phase composition as well as the Bi/Mo ratios determined by ICP-OES and XPS are summarized in Table 2. For the sample synthesized with a Bi/Mo ratio 2:1 additionally to γ-Bi_2MoO_6 the β-phase was formed during calcination at 550 °C. The presence of β-$Bi_2Mo_2O_9$ is indicated by characteristic reflections at 27.9° and 31.8° in the diffraction pattern in Figure 6a and by the band at 885 cm^{-1} in the Raman spectrum (Figure 6b). As the β-phase is considered stable between 540 and 665 °C, formation of β-$Bi_2Mo_2O_9$ was also expected for the calcined sample emerging from Bi/Mo = 1:1. Surprisingly, calcination of HT_Bi1Mo1 only improved the crystallinity of the α- and γ-bismuth molybdate mixture, but did not lead to the formation of β-$Bi_2Mo_2O_9$. This suggests that higher calcination temperatures or longer treatment times should have been applied and according investigations are under way. Li et al. [8] could not synthesize the β-phase directly by hydrothermal synthesis but after calcination at 560 °C. Beale and Sankar [25] showed by combined EDXRD/XAS that phase-pure β-$Bi_2Mo_2O_9$ could be produced from a hydrothermally synthesized precursor material by heat treatment at temperatures above 500 °C.

After calcination at 550 °C for 4 h the sample synthesized from a Bi/Mo ratio 2:3 only contained α-$Bi_2Mo_3O_{12}$. HT_Bi1Mo2_calc containing a larger excess of molybdenum additionally showed characteristic features of α-MoO_3 in the diffraction pattern (Figure 6a; reflections at 23.3°, 25.7°, 27.3°, 33.7°) and in the Raman spectra (Figure 6b; 993 cm^{-1}). Bi/Mo ratios found in the bulk of the

products synthesized with Bi/Mo = 2:1 and 2:3 were consistent with the applied ratio and did not change during calcination (Table 2), thereby indicating that no molybdenum or bismuth losses occurred during thermal treatment. Comparison of the metal ratio in the bulk determined by ICP-OES and on the surface (XPS) showed that both values were practically identical after calcination. The surface composition of the catalyst was determined from the peak areas of Mo $3d_{5/2}$ = 232.7 eV and Bi $4f_{7/2}$ = 159.5 eV and a representative spectrum is shown in the supporting information. XPS measurement of the as prepared HT_Bi2Mo1 revealed enrichment with bismuth on the surface, which might be due to the presence of $Bi_2O_{3.96}$. However, the activity for propylene conversion was sufficiently high and no formation of hexadiene due to the presence of Bi_2O_3 could be observed [38, 39]. Hence, it is more likely that the γ-bismuth molybdates have an excess of superficial bismuth, which is in line with literature [20, 42]. Bing et al. [12] also observed a decrease of the surface Bi/Mo ratio for γ-Bi_2MoO_6 prepared by co-precipitation during calcination at 420 °C. van Well et al. [21] calcined spray dried and co-precipitated samples with a theoretical Bi/Mo ratio of 2.0 at 550 °C and determined similar surface ratios to the values found for our hydrothermally synthesized samples: the high Bi/Mo ratio of 3.0 determined for the as prepared HT_Bi2Mo1 and the value of 1.9 for the calcined sample containing additional amounts of the β-phase (see Table 2).

3.2.2. Catalytic performance before and after calcination.

Next, the four calcined samples HT_Bi2Mo1_calc, HT_Bi1Mo1_calc, HT_Bi2Mo3_calc and HT_Bi1Mo2_calc were applied in the catalytic oxidation of propylene where they exhibited a lower propylene conversion and, accordingly, a lower acrolein yield than the non-calcined samples under the same conditions (flow range 50 – 260 Nml/min, 460 – 520 °C). Figure 7 compares the acrolein yield and the propylene conversion of the as prepared and calcined catalysts at 480 °C and 120 Nml/min. The acrolein yield for the calcined samples decreased with increasing molybdenum content to 1.0% at corresponding propylene conversion of 1.7% for HT_Bi1Mo2_calc.

For HT_Bi2Mo3 propylene conversion decreased from 15.8% to 2.3% due to calcination and the acrolein selectivity increased from 82% to 92%. Comparing the phase composition of this sample

before and after calcination suggests that the phase change was responsible for the deactivation. The ammonium molybdenum oxide phase in HT_Bi2Mo3 was removed in the course of calcination and phase pure α-$Bi_2Mo_3O_{12}$ was obtained (Figure 7). This ammonium molybdenum phase should have a lower catalytic activity in propylene oxidation and a lower selectivity to acrolein than α-$Bi_2Mo_3O_{12}$ [13]. Therefore the mixture of ammonium molybdenum oxide and α-$Bi_2Mo_3O_{12}$ should be less active and less selective than pure α-$Bi_2Mo_3O_{12}$. However, calcination of the other three samples also led to a deactivation in propylene oxidation. For HT_Bi2Mo1 the β-phase was formed and for HT_Bi1Mo2 hexagonal $NH_3(MoO_3)_3$ was changed to orthorhombic MoO_3. HT_Bi1Mo1 did not undergo phase changes during calcination but the deactivation through thermal treatment was more significant than for the other three samples. Although propylene conversion decreased for the calcined samples compared to the as prepared materials, the selectivity decreased only for HT_Bi1Mo1 and HT_Bi1Mo2. For HT_Bi2Mo1 and HT_Bi2Mo3 acrolein selectivity increased from 69 to 80% and from 82 to 92% but the resulting acrolein yield was always lower for the calcined than the as-prepared sample.

van Well et al. [21] reported that calcination time and temperature strongly influenced the activity of the bismuth molybdenum catalysts. They proposed surface enrichment with bismuth after calcination at higher temperature or longer time as an explanation. This hypothesis could not be confirmed here, because the bismuth concentration on the surface decreased during calcination (see Table 2). A direct correlation between the Bi/Mo ratio on the surface given in Table 1 and the corresponding propylene conversion could thus not be derived. An alternative explanation could be the decrease of the surface area, which was ≤ 1 m^2/g for all calcined samples, leading to low propylene conversion.

Comparison of SEM images in Figure 8 and Figure 2 revealed that the particles sinter and agglomerate during calcination. Only the sample prepared from an initial Bi/Mo ratio 2:1 retained a plate-like morphology, but the thickness increased during calcination and the aspect ratio changed from rectangular to quadratic (Figure 8a). In summary, only HT_Bi2Mo1 partially preserved its

morphology during calcination and this sample showed the best catalytic performance compared to the other three calcined materials.

3.3. Comparison of different hydrothermally prepared catalysts with co-precipitated bismuth molybdates.

3.3.1. Characterization of hydrothermally prepared and conventionally synthesized catalysts.

The diffraction patterns of the bismuth molybdate samples prepared from different Bi/Mo ratios by hydrothermal synthesis or co-precipitation are shown in Figure 9. Samples prepared with a Bi/Mo ratio 2:1 all contained mainly γ-Bi_2MoO_6 except for the co-precipitated sample calcined at 680 °C, which consisted of γ”-Bi_2MoO_6, whereas α-$Bi_2Mo_3O_{12}$ was the main phase for Bi/Mo = 2:3. The samples prepared with Bi/Mo = 1:1 consisted of a mixture of the α-phase with either β- or γ-bismuth molybdate.

As already discussed in section 3.1, hydrothermal synthesis at 180 °C with Bi/Mo = 2:1 prepared in pure water led to the formation of γ-Bi_2MoO_6 with some other Mo- or Bi-containing phases as impurity. Addition of acetic acid did also result in the formation of γ-Bi_2MoO_6, albeit with α-$Bi_2Mo_3O_{12}$ as a side product. This sample featured agglomerates of flat plates with round-shaped edges illustrated in Figure 10a and b. Phase pure γ-Bi_2MoO_6 was obtained from synthesis in the presence of nitric acid. The plates of HT_Bi2Mo1_HNO3 (Figure 10c) were rectangular with well defined steps and edges on the surface, which may be beneficial for the selectivity of the catalytic reaction. Co-precipitation followed by calcination at 450 °C yielded pure γ-Bi_2MoO_6 as well, whereas γ”-Bi_2MoO_6 (PDF No. 33-208 [31]) [9] was formed during calcination at 680 °C as indicated by the reflections at 27.4, 31.1, 31.9 and 45.1°. Hydrothermal synthesis with Bi/Mo = 1:1 did not lead to the formation of the β-phase but to a mixture of α- and γ-phase for all three samples. Co-precipitation of bismuth molybdates with Bi/Mo = 1:1 and calcination at 680 °C resulted in a mixture of β-$Bi_2Mo_2O_9$ and α-$Bi_2Mo_3O_{12}$.

N_2 physisorption measurements showed that the co-precipitated samples and the hydrothermally synthesized samples exhibited similar surface areas (6 - 9 m^2/g; cf. Table 3).

The Bi/Mo ratios determined by ICP-OES and XPS are summarized in Table 3. For both preparation methods the applied ratio corresponded to the bulk concentration actually present in the prepared catalyst. A loss of molybdenum, which was found by van Well et al. [21] during precipitation, could not be confirmed here, probably because higher pH values were applied in the present study. Comparison of the ICP-OES results with the corresponding ratios calculated from XPS shows that the samples containing γ-Bi_2MoO_6 exhibit an excess of bismuth on the surface. HT_Bi2Mo1 displayed the highest Bi excess, whereas heat treatment (e.g. calcination of the co- precipitated samples) led to a reduced Bi/Mo ratio on the surface (Table 3).

3.3.2. Catalytic performance comparison of hydrothermally synthesized and co-precipitated samples.

The catalytic performance of all materials during the selective oxidation of propylene to acrolein at 320 °C and 360 °C is summarized in Figure 11. At 320 °C the co-precipitated sample synthesized with Bi/Mo = 2:1 which consisted of γ-Bi_2MoO_6 showed the highest catalytic activity with propylene conversion of 5 - 11% at acrolein selectivities of 59 – 69%. HT_Bi2Mo1 which additionally to γ-Bi_2MoO_6 contained α-$Bi_2Mo_3O_{12}$ also exhibited relatively high propylene conversion (3 – 9%) at acrolein selectivities of 58 – 100%. In Figure 11b the catalytic activities are reported for the surface area inside the reactor instead for a fixed weight of catalyst as in Figure 11a. Comparison of these two figures shows that the catalytic activities of the different samples still follow the same trend except CP_Bi2Mo3_450. The co-precipitated sample synthesized with Bi/Mo = 2:3 exhibited higher propylene conversion per surface area than the other bismuth molybdates due to its low surface area (1 m^2/g). The two samples calcined at 680 °C (CP_Bi1Mo1_680 and CP_Bi2Mo1_680) with surface areas < 1 m^2/g showed very low catalytic activity in the selective oxidation of propylene and also low propylene conversion per surface area at 320 °C (Figure 11a and b). An increase in reaction temperature to 360 °C resulted in higher propylene conversion for all samples (up to 27%) and

acrolein selectivities of mainly 60 – 70%. Comparison of the samples synthesized with the ratio Bi/Mo = 2:1 evidenced that the samples HT_Bi2Mo1_HNO3 and CP_Bi2Mo1_450, both synthesized using nitric acid and consisting of pure γ-Bi_2MoO_6 showed the highest activity, whereas the co-precipitated sample was less selective than the hydrothermally synthesized sample. This difference in selectivity could be associated with the morphology, which was well defined for HT_Bi2Mo1_HNO3 but random for co-precipitated samples [43, 44]. The samples synthesized under hydrothermal conditions with acetic acid, which partially led to the formation of α-$Bi_2Mo_3O_{12}$, showed relatively low activity in propylene oxidation and low selectivity for acrolein. In general, Figure 11c suggests that the γ-phase was more active than the α-phase as the two most active samples consisted only of γ-Bi_2MoO_6. The two samples synthesized with nitric acid but different Bi/Mo ratios (HT_Bi2Mo1_HNO3 and HT_Bi1Mo1_HNO3) both showed relatively high catalytic activity but HT_Bi1Mo1_HNO3, containing a mixture of α-$Bi_2Mo_3O_{12}$ and γ-Bi_2MoO_6, was slightly less active and selective than HT_Bi2Mo1_HNO3. In Figure 11d acrolein selectivity is given as a function of propylene conversion per surface area. CP_Bi2Mo1_450 and HT_Bi2Mo1_HNO3 still exhibited high propylene conversion per surface area but again the co-precipitated sample synthesized with Bi/Mo = 2:3 obtained the highest values for propylene conversion per surface area (5 – 10.4 %/m²) due to the low surface area of this sample (1 m²/g). Also at 360 °C both samples calcined at 680 °C (CP_Bi2Mo1_680 and CP_Bi1Mo1_680) were inactive for propylene oxidation, due to the high temperature treatment and the very low surface area (< 1 m²/g). As calcination at 550 °C strongly decreased the surface area and the activity of the prepared samples without affording β-$Bi_2Mo_2O_9$, prolonged calcination at higher temperatures would probably not exert a productive influence either. Whereas direct hydrothermal synthesis of β-$Bi_2Mo_2O_9$ without calcination was not possible, the obtained mixtures (HT_Bi1Mo1, HT_Bi1Mo1_HNO3, HT_Bi1Mo1_pH4) still exhibited relatively high activity at 360 °C.

According to Table 3, where the maximum acrolein yield for each sample and the corresponding propylene conversion are summarized, HT_Bi1Mo1_pH4, HT_Bi1Mo1_HNO3 and HT_Bi2Mo1_HNO3, i.e. the samples synthesized under hydrothermal conditions with nitric acid or ammonia, were the

most active catalysts. One reason for this superior performance could be the incorporation of nitrogen in the catalyst, but the analysis of the nitrogen content of the samples HT_Bi2Mo1, HT_Bi2Mo1_HOAc and HT_Bi2Mo1_HNO3 resulted in 0.4 wt.%, 0.1 wt.% and 0.1 wt.% N and does not correlate with the catalytic performance. The highest nitrogen content was found for the sample synthesized in the absence of acid, probably due to the presence of a nitrate phase, which disappeared during calcination. HT_Bi2Mo1_HOAc, which is composed of γ-Bi_2MoO_6 and α-$Bi_2Mo_3O_{12}$, also contained nitrogen. This indicated that either the Mo or the Bi precursor or both acted as main nitrogen source instead of HNO_3 or NH_3. The increased activity of the samples synthesized with nitric acid could not be explained in terms of nitrogen incorporation but by the difference in phase composition and morphology due to the different acids applied (no acid, acetic acid or nitric acid). Addition of a strong inorganic acid (nitric acid) resulted in different particle morphology compared to a weak organic acid (acetic acid; cf. Figure 10) and therefore the catalytic performance of the resulting bismuth molybdate was different.

A direct correlation of the Bi/Mo ratio on the surface determined by XPS (see Table 3) with propylene conversion and acrolein yield was not possible. Hence, the phase composition and the surface area of the samples determine their catalytic performance. Comparison of the samples HT_Bi2Mo1_HNO3 and HT_Bi1Mo1_HNO3 demonstrated that the catalytic performance of these two samples was identical at 360 °C although they showed different phase composition. A synergistic effect between the α- and the γ-phase could not be confirmed comparing HT_Bi1Mo1_HNO3 to HT_Bi2Mo1_HNO3, which only contained γ-Bi_2MoO_6.

Comparison of the catalytic performance of the co-precipitated samples calcined at 450 °C showed that γ-Bi_2MoO_6 (CP_Bi2Mo1_450) converted more propylene and yielded more acrolein than α-$Bi_2Mo_3O_{12}$ (CP_Bi2Mo3_450). Generally, comparison of catalysts prepared under the same conditions shows that the activity decreased in the following order: γ-Bi_2MoO_6 > α-$Bi_2Mo_3O_{12}$. However, a different order of activity has been suggested in preceding studies, namely: β-$Bi_2Mo_2O_9$ ≥ α-$Bi_2Mo_3O_{12}$ > γ-Bi_2MoO_6 [2, 45-47]. Krenzke and Keulks [48] as well as Batist et al. [49] observed yet

another trend (γ-Bi_2MoO_6 ≥ β-$Bi_2Mo_2O_9$ > α-$Bi_2Mo_3O_{12}$), confirming the α-phase as the least active phase.

CP_Bi2Mo1_680 changed its phase composition from metastable γ"-Bi_2MoO_6 to a mixture of orthorhombic γ´-Bi_2MoO_6 and γ-Bi_2MoO_6. This transformation usually occurs between 550 – 640 °C [9, 10]. Except CP_Bi2Mo1_680, HT_Bi2Mo1 and HT_Bi2Mo3 (cf. section 3.1) all other samples were stable during the activity measurements up to 520 °C (see powder X-ray diffraction pattern in Figure S3 Supporting Information).

For the highly active HT_Bi2Mo1_HNO3 propylene conversion and acrolein selectivity was measured at two different oxygen concentrations (5% O_2 with $C_3H_6/O_2/N_2$ = 5/5/90 and 25% O_2 with $C_3H_6/O_2/N_2$ = 5/25/70; see Fig. S4 in ESI) which evidenced that at 320 °C and 360 °C the catalytic performance (activity and selectivity) was strongly influenced by the oxygen concentration present in the reaction gas. Higher oxygen concentration (25%) resulted in higher propylene conversion and lower acrolein selectivity. At 400 °C and 440 °C propylene conversion was independent of the oxygen concentration. This indicates that at temperatures below 400 °C reoxidation of the catalyst is the rate determining step. Comparison of the XP spectra of some representative samples before and after the catalytic test measurements did not result in a shift of the binding energies for bismuth (159.5 eV) and molybdenum (232.6 eV) indicating that bismuth is present as Bi^{3+} [50] and molybdenum as Mo^{6+} [51] before and after the catalytic test reaction. This shows that the used catalyst was completely reoxidized (see Fig. S5 in ESI), which was also demonstrated in air [27]. The Bi/Mo ratio on the surface of the used samples were lower than the corresponding ratio of the fresh bismuth molybdates (cf. Table 3 and Figure S5 Supporting Information) which can be explained by the relatively high temperatures in the reactor (up to 520 °C; cf. 3.3.1). XPS of the used catalysts also proofed that coke formation on these bismuth molybdates can be neglected as the carbon amount on the surface of the catalyst before and after the catalytic tests did only differ in the range of the measurement inaccuracy.

4. Conclusion

The catalytic performance of bismuth molybdates strongly depends on the crystalline phases present in the catalysts and their morphologies which emerge from the selected synthetic method. During hydrothermal synthesis application of a high Bi/Mo ratio led mainly to the formation of γ-Bi_2MoO_6, while applying a Bi/Mo ratio < 1 resulted in α-$Bi_2Mo_3O_{12}$ as the main phase. A mixture of α- and γ-phase was obtained with precursor ratios of Bi/Mo = 1:1. As hydrothermal synthesis did not provide access to the one-step formation of β-$Bi_2Mo_2O_9$ under the parameters applied in the present study, the materials synthesized in pure water were furthermore calcined at 550 °C. Even these harsh conditions resulted only in partial formation of the β-phase, and the process can probably be driven to completion only at the expense of considerable loss of surface area and catalytic performance. The catalytic activity of the freshly hydrothermally prepared catalysts was significantly higher than after their calcination at 550°C. Furthermore, the obtained acrolein yield decreased regardless of the phase composition. Generally, for the investigation of the relative activities of the different bismuth molybdate phases catalysts should be prepared under the same conditions including pre-conditioning of the precursor materials. Therefore we used as prepared materials or applied the same heat treatment to compare the catalytic performance of the different bismuth molybdate phases. In addition, highly active catalysts could be prepared under hydrothermal conditions applying initial Bi/Mo ratios of 1:1 or 2:1 with nitric acid or ammonia as additives. Generally, these catalysts were more selective at comparable propylene conversion than co-precipitated γ-Bi_2MoO_6. Consequently, extension of this method to industrially more relevant Bi-Mo-O systems containing, e.g. Co, Fe or V as additional elements is a promising concept.

ACKNOWLEDGMENTS

We thank the Danish Research Council for financial support in the framework of the DSF proposal "Nanoparticle synthesis for catalysis". We gratefully acknowledge Hermann Köhler at the Institute of Catalysis Research and Technology (IKFT) at KIT for performing ICP-OES measurements and Dr. Thomas Bergfeldt at the Institute for Applied Materials in the Chemical Analysis group (IAM-AWP) at

KIT for the quantitative nitrogen analysis. The Center for Electron Nanoscopy (CEN) at DTU is gratefully acknowledged for the possibility to use the scanning electron microscopes (SEM) and the help and support during the measurements. G. R. P. acknowledges financial support by the Swiss National Science Foundation (SNSF Professorship PP00P2-13348/1) and by the University of Zurich.

Electronic supporting information:

The supporting information contains a representative XPS (before and after use), Raman spectra of samples prepared by hydrothermal synthesis and co-precipitation. Moreover, powder X-ray diffraction patterns of the samples before and after application in selective oxidation (cf. section 3.3) and the catalytic performance in the selective oxidation of propylene at different oxygen concentrations are reported.

References

[1] J.L. Callahan, R.K. Grasselli, E.C. Milberge, H.A. Strecker, Erdöl und Kohle Erdgas, Petrochem. 24 (1971) 349.
[2] R.K. Grasselli, J.D. Burrington, Adv. Catal. 30 (1981) 133-163.
[3] Y. Morooka, W. Ueda, Adv. Catal. 40 (1994) 233-273.
[4] L.D. Krenzke, G.W. Keulks, J. Catal. 64 (1980) 295-302.
[5] W. Ueda, Y. Morooka, T. Ikawa, I. Matsuura, Chem. Lett. (1982) 1365-1368.
[6] S.R.G. Carrazán, C. Martin, V. Rives, R. Vidal, Appl. Catal., A. 135 (1996) 95-123.
[7] D.H. He, W. Ueda, Y. Morooka, Catal. Lett. 12 (1992) 35-44.
[8] H. Li, K. Li, H. Wang, Mater. Chem. Phys. 116 (2009) 134-142.
[9] D.J. Buttrey, T. Vogt, U. Wildgruber, W.R. Robinson, J. Solid State Chem. 111 (1994) 118-127.
[10] D.J. Buttrey, D.A. Jefferson, J.M. Thomas, Philos. Mag. A. 53 (1986) 897-906.
[11] J.R. Monnier, G.W. Keulks, J. Catal. 68 (1981) 51-66.
[12] Z. Bing, S. Pei, S. Shishan, G. Xiexian, J. Chem. Soc., Faraday Trans. 86 (1990) 3145-3150.
[13] J.D. Burrington, R.K. Grasselli, J. Catal. 59 (1979) 79-99.
[14] D. Carson, M. Forissièr, J.C. Védrine, J. Chem. Soc., Faraday Trans. 1. 80 (1984) 1017-1028.
[15] M.T. Le, W.J.M. van Well, P. Stoltze, I. van Driessche, S. Hoste, Appl. Catal., A. 282 (2005) 189-194.
[16] G.W. Keulks, J.L. Hall, C. Daniel, K. Suzuki, J. Catal. 34 (1974) 79-97.
[17] F. Trifiro, R.D. Scarle, H. Hoser, J. Catal. 25 (1972) 12.
[18] R.P. Rastogi, A.K. Singh, C.S. Shukla, J. Solid State Chem. 42 (1982) 136-148.
[19] L.M. Thang, L.H. Bac, I. van Driessche, S. Hoste, W.J.M. van Well, Catal. Today. 131 (2008) 566-571.
[20] M.T. Le, J. Van Craenenbroeck, I. Van Driessche, S. Hoste, Appl. Catal., A. 249 (2003) 355-364.
[21] W.J.M. van Well, M.T. Le, N.C. Schiodt, S. Hoste, P. Stoltze, J. Mol. Catal. A: Chem. 256 (2006) 1-8.
[22] J.Q. Yu, A. Kudo, Chem. Lett. 34 (2005) 1528-1529.
[23] H. Kodama, F. Izumi, J. Cryst. Growth. 50 (1980) 515-520.
[24] K. Zheng, Y. Zhou, L. Gu, X. Mo, G.R. Patzke, G. Chen, Sens. Actuators, B. 148 (2010) 240-246.
[25] A.M. Beale, G. Sankar, Chem. Mater. 15 (2003) 146-153.
[26] K.L. Parry, A.G. Shard, R.D. Short, R.G. White, J.D. Whittle, A. Wright, Surf. Interface Anal. 38 (2006) 1497-1504.

[27] J.-D. Grunwaldt, M.D. Wildberger, T. Mallat, A. Baiker, J. Catal. 177 (1998) 53-59.
[28] A. Ayame, K. Uchida, M. Iwataya, M. Miyamoto, Appl. Catal., A. 227 (2002) 7-17.
[29] J.H. Scofield, J. Electron. Spectrosc. Relat. Phenom. 8 (1976) 129-137.
[30] M. Høj, A.D. Jensen, J.-D. Grunwaldt, Appl. Catal., A. 451 (2013) 207-215.
[31] http://icsd.fiz-karlsruhe.de/ (October 2013).
[32] F. Pertlik, J. Zemann, Fortschr. Mineral. 60 (1982) 162-163.
[33] B. Begemann, M. Jansen, J. Less. Common Met. 156 (1989) 123-135.
[34] A.N. Christensen, M.-A. Chevallier, J. Skibsted, B.B. Iversen, J. Chem. Soc. Dalton (2000) 265-270.
[35] F. Theobald, A. Laarif, A.W. Hewat, Ferroelectr. 56 (1984) 219-237.
[36] F.D. Hardcastle, I.E. Wachs, J. Phys. Chem. 95 (1991) 10763-10772.
[37] R.P. Oertel, R.A. Plane, Inorg. Chem. 7 (1968) 1192-1196.
[38] B. Grzybowska, J. Haber, J. Janas, J. Catal. 49 (1977) 150-163.
[39] H.E. Swift, J.E. Bozik, J.A. Ondrey, J. Catal. 21 (1971) 212.
[40] E. Vila, A.R. Landa-Canovas, J. Galy, J.E. Iglesias, A. Castro, J. Solid State Chem. 180 (2007) 661-669.
[41] P.J. Bereciartua, F.J. Zuniga, J.M. Perez-Mato, V. Petricek, E. Vila, A. Castro, J. Rodriguez-Carvajal, S. Doyle, Acta Crystallogr., Sect. B: Struct. Sci. 68 (2012) 323-340.
[42] J.M. Herrmann, M. Eljamal, M. Forissier, React. Kinet. Catal. Lett. 37 (1988) 255-260.
[43] M.T. Le, W.J.M. van Well, I. van Driessche, S. Hoste, Can. J. Chem. Eng. 83 (2005) 336-343.
[44] A.P.V. Soares, L.D. Dimitrov, M. de Oliveira, L. Hilaire, M.F. Portela, R.K. Grasselli, Appl. Catal., A. 253 (2003) 191-200.
[45] J.F. Brazdil, D.D. Suresh, R.K. Grasselli, J. Catal. 66 (1980) 347-367.
[46] E. Godard, E.M. Gaigneaux, P. Ruiz, B. Delmon, Catal. Today. 61 (2000) 279-285.
[47] I. Matsuura, R. Schut, K. Hirakawa, J. Catal. 63 (1980) 152-166.
[48] L.D. Krenzke, G.W. Keulks, J. Catal. 61 (1980) 316-325.
[49] P.A. Batist, J.F.H. Bouwens, G.C.A. Schuit, J. Catal. 25 (1972) 1.
[50] L. Chen, E. Aarcon-Lado, M. Hettick, I.D. Sharp, Y. Lin, A. Javey, J.W. Ager, J. Phys. Chem. C. 117 (2013) 21635-21642.
[51] J.G. Choi, L.T. Thompson, Appl. Surf. Sci. 93 (1996) 143-149.

Tables

Table 1: Characterization of hydrothermally prepared samples with different Bi/Mo ratios before and after the catalytic tests by PXRD, Raman spectroscopy and BET (main phases in bold letters).

Sample	Phases according to PXRD		Phases according to Raman spectroscopy		Specific surface area (BET) [m^2/g]
	as-prepared	after use	as-prepared	after use	as-prepared
HT_Bi3Mo1	**γ-Bi_2MoO_6**, cubic BiO_{2-x}	**γ-Bi_2MoO_6**, $Bi_8Mo_3O_{21}$	**γ-Bi_2MoO_6**	**γ-Bi_2MoO_6**, γ´-Bi_2MoO_6	30
HT_Bi2Mo1	**γ-Bi_2MoO_6**, α-$Bi_2Mo_3O_{12}$, $Bi_6O_6(OH)_3(NO_3)_3 \cdot 1.5H_2O$	**γ-Bi_2MoO_6**	**γ-Bi_2MoO_6**, presence of NO_3^-	**γ- Bi_2MoO_6**	6
HT_Bi1Mo1	**γ-Bi_2MoO_6** and **α-$Bi_2Mo_3O_{12}$**	**γ-Bi_2MoO_6** and **α-$Bi_2Mo_3O_{12}$**	**α-$Bi_2Mo_3O_{12}$**	n.d.	8
HT_Bi2Mo3	**α-$Bi_2Mo_3O_{12}$**, cubic $H_{0.68}(NH_4)_2Mo_{14.16}O_{4.34} \cdot 6.92H_2O$	**α-$Bi_2Mo_3O_{12}$**	**α-$Bi_2Mo_3O_{12}$**, MoO_3	**α-$Bi_2Mo_3O_{12}$**	7
HT_Bi1Mo2	**α-$Bi_2Mo_3O_{12}$**, hexagonal $NH_3(MoO_3)_3$	**α-$Bi_2Mo_3O_{12}$**, α-MoO_3	**α-$Bi_2Mo_3O_{12}$**, $NH_3(MoO_3)_3$	α-**$Bi_2Mo_3O_{12}$**, MoO_3	6

Table 2: Characterization of hydrothermally prepared samples before and after calcination at 550 °C for 4 h. Phases were identified by PXRD, the ratio of bismuth to molybdenum in the bulk and on the surface were calculated from ICP-OES (atom %) and XPS analysis.

Sample	Phases according to PXRD			Bi/Mo ratio bulk		Bi/Mo ratio surface	
	as-prepared	Calcined at 550°C for 4 h	Calcined and used	as-prep.	calc	as-prep.	calc
HT_Bi2Mo1	**γ-Bi_2MoO_6**, α-$Bi_2Mo_3O_{12}$, $Bi_6O_6(OH)_3(NO_3)_3 \cdot 1.5H_2O$	**γ-Bi_2MoO_6**, some β-$Bi_2Mo_2O_9$	**γ-Bi_2MoO_6**	2.0	2.0	3.0	1.9
HT_Bi1Mo1	**γ-Bi_2MoO_6** and **α-$Bi_2Mo_3O_{12}$**	**γ-Bi_2MoO_6** and **α-$Bi_2Mo_3O_{12}$**	**γ-Bi_2MoO_6** and **α-$Bi_2Mo_3O_{12}$**	n.d.	n.d.	1.3	n.d.
HT_Bi2Mo3	**α-$Bi_2Mo_3O_{12}$**, cubic $H_{0.68}(NH_4)_2Mo_{14.16}O_{4.34} \cdot 6.92H_2O$	**α-$Bi_2Mo_3O_{12}$**	**α-$Bi_2Mo_3O_{12}$**	0.7	0.7	0.8	0.7
HT_Bi1Mo2	**α-$Bi_2Mo_3O_{12}$**, hexagonal $NH_3(MoO_3)_3$	**α-$Bi_2Mo_3O_{12}$**, MoO_3	**α-$Bi_2Mo_3O_{12}$**, MoO_3	0.5	n.d.	n.d.	n.d.

Table 3: Characterization and catalytic data of the differently prepared samples. All samples are as-prepared and non-calcined except the co-precipitated samples (calcination temperature is included in the sample name).

Sample	Maximum yield (C_3H_4O)	Corresponding Conversion (C_3H_6)	T	Specific surface area (BET)	Bi/Mo ratio bulk [a]	Bi/Mo ratio surface [b]	
	[at.%/at.%]					[at.%/at.%]	
	%	%	°C	[m²/g]	fresh	fresh	used
CP_Bi2Mo1_450	25.3	33.9	491	6	2.0	2.3	2.1
CP_Bi2Mo1_680	5.8	7.3	482	< 1	n.d.	n.d.	n.d.
HT_Bi2Mo1_HNO3	33.6	41.2	450	6	1.8	2.8	1.9
HT_Bi2Mo1_HOAc	20.1	26.8	405 [c]	5	n.d.	n.d.	n.d.
HT_Bi2Mo1	23.1	33.3	445	6	2.0	3.0	2.6
CP_Bi1Mo1_680	3.6	4.3	521	< 1	n.d.	n.d.	n.d.
HT_Bi1Mo1_HNO3	38.4	43.8	486	9	n.d.	1.2	1.1
HT_Bi1Mo1_pH4 [d]	36.6	45.5	489	7	n.d.	n.d.	n.d.
HT_Bi1Mo1	31.0	39.9	493	8	n.d.	1.3	n.d.
CP_Bi2Mo3_450	15.3	18.8	483	1	0.7	n.d.	n.d.
HT_Bi2Mo3	21.9	28.9	443	7	0.7	0.8	0.7

a: The calculated error accounts to around 10%

b: Average of two XPS measurements at different spots

c: Maximum test temperature 400 °C for HT_Bi2Mo1_HOAc

d: pH value adjusted with NH_3

Figures

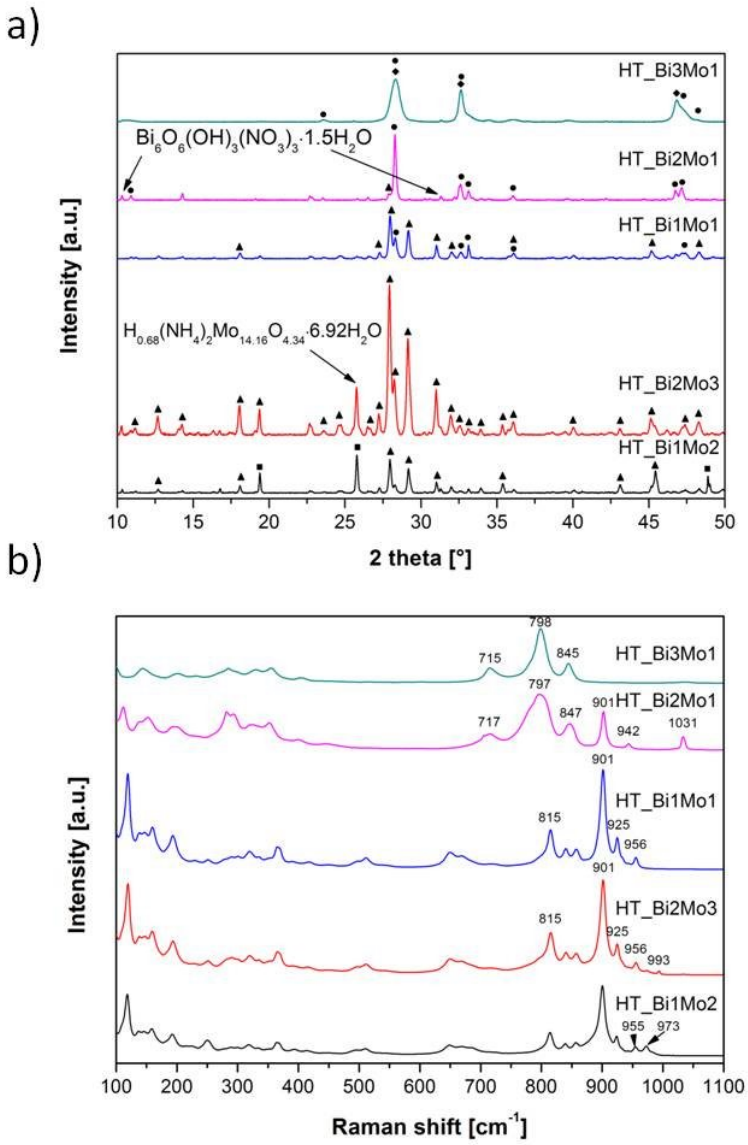

Figure 1: Characterization of the samples prepared with different Bi/Mo ratio under hydrothermal conditions without calcination by X-ray diffraction (a) and Raman spectroscopy (b). The different phases in pattern (a) are indicated as follows: α-$Bi_2Mo_3O_{12}$ (triangles), γ-Bi_2MoO_6 (circles), $NH_3(MoO_3)_3$ (squares), BiO_{2-x} (diamond).

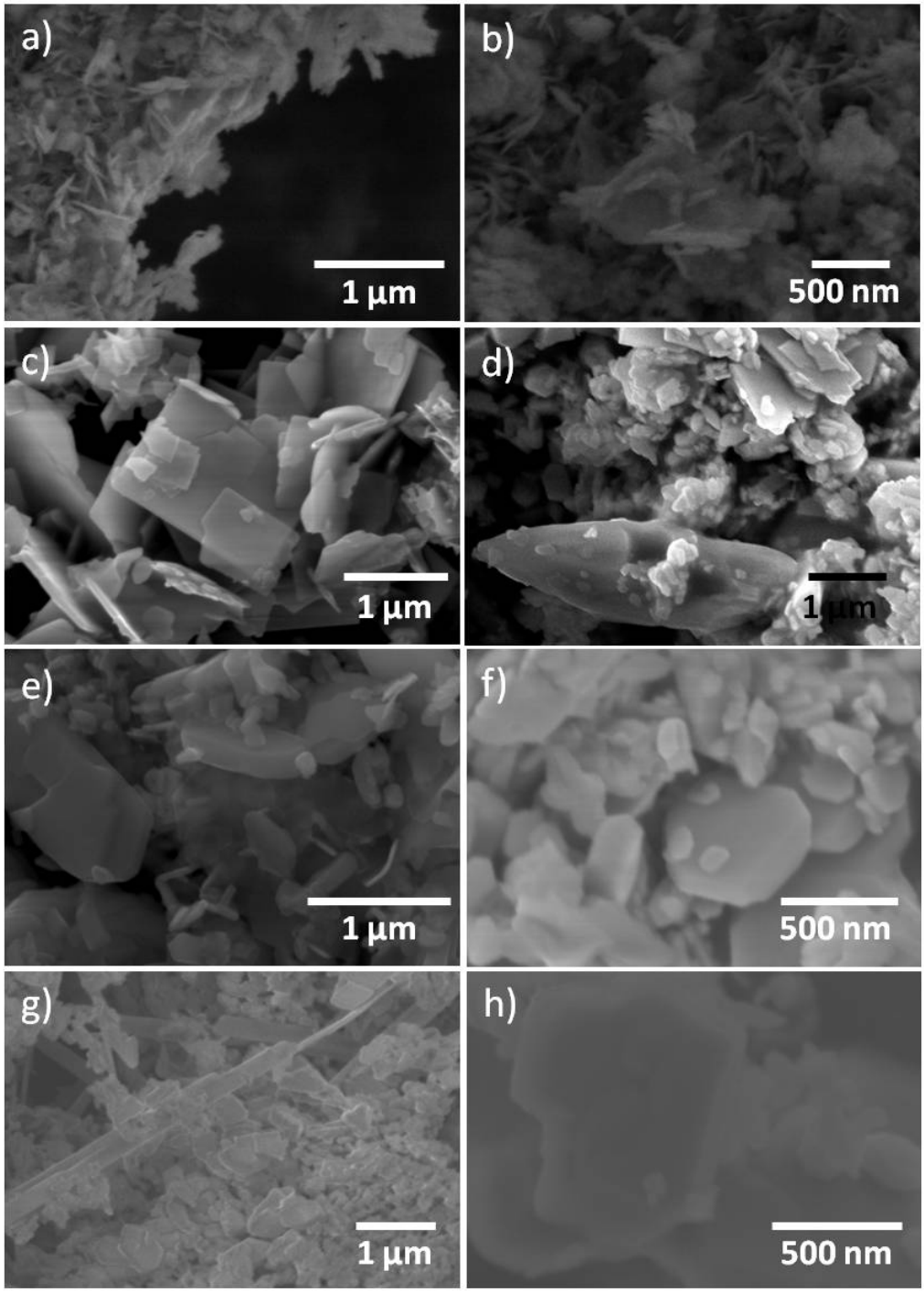

Figure 2: SEM images of hydrothermally synthesized samples with different Bi/Mo ratio without further calcination a-b) HT_Bi3Mo1, c) HT_Bi2Mo1, d) HT_Bi1Mo2, e-f) HT_Bi1Mo1, g-h) HT_Bi2Mo3.

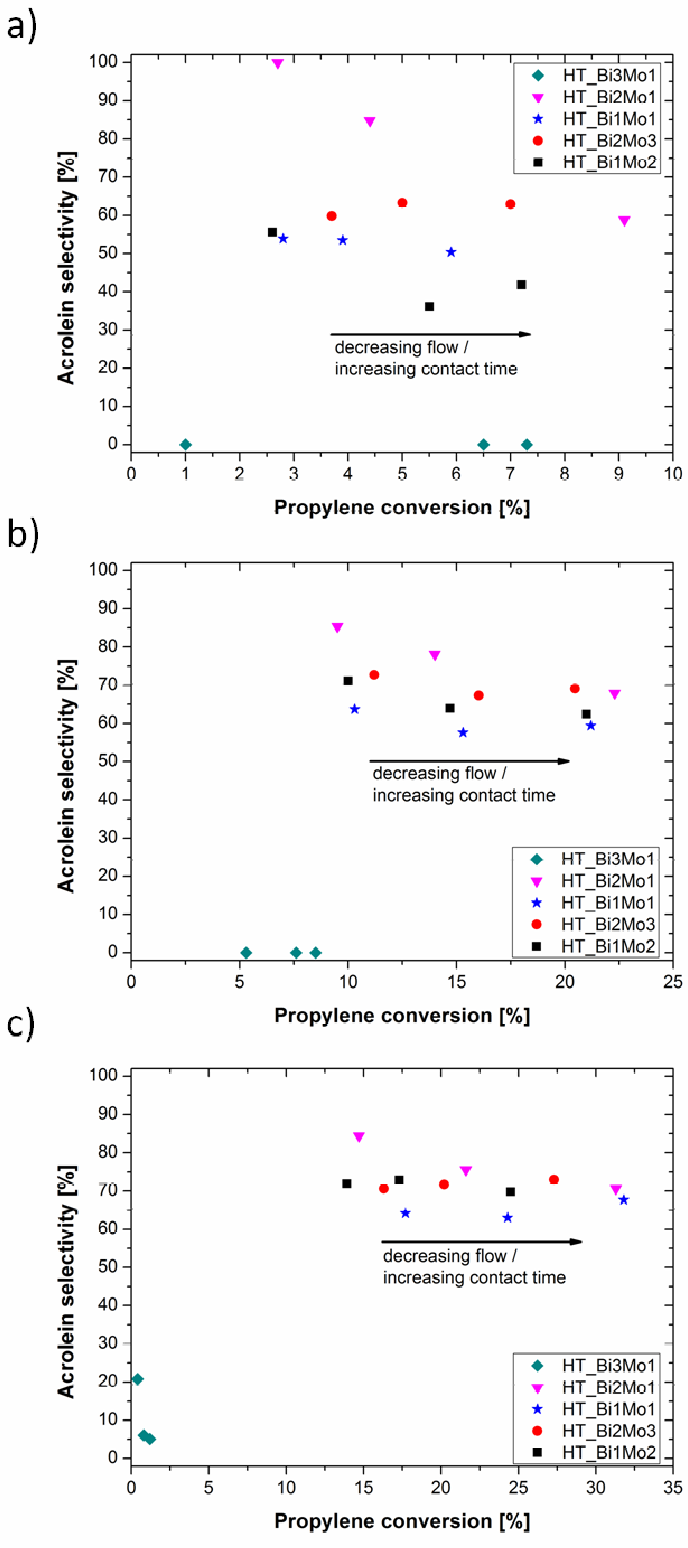

Figure 3: Catalytic performance of hydrothermally prepared samples with different Bi/Mo ratios at 320 °C (a) 360 °C (b) and 400 °C (c) without calcination. 500 mg of the as prepared samples (150 – 300 µm) were pre-treated in the reactor in synthetic air at 300°C and the catalytic performance was measured using a gas composition of $C_3H_6/O_2/N_2$ = 5/25/70 and flows of 50, 80, 120 Nml/min.

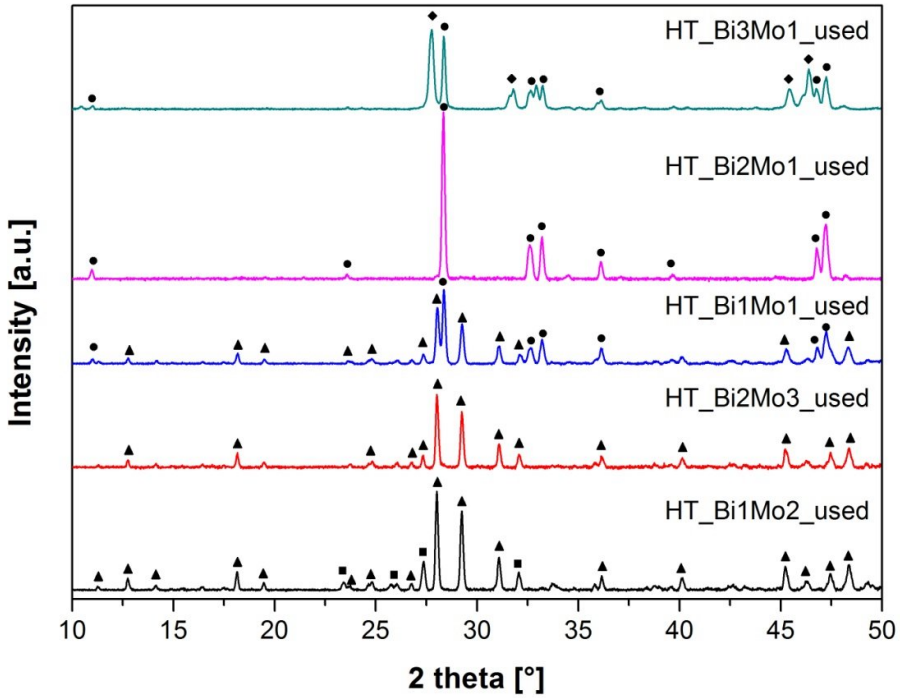

Figure 4: PXRD pattern of hydrothermally synthesized samples after propylene oxidation at temperatures up to 520 °C, illustrating that no major changes occurred in the main phase after catalysis; α-$Bi_2Mo_3O_{12}$ (triangles), γ-Bi_2MoO_6 (circles), α-MoO_3 (squares) and $Bi_8Mo_3O_{21}$ (diamond).

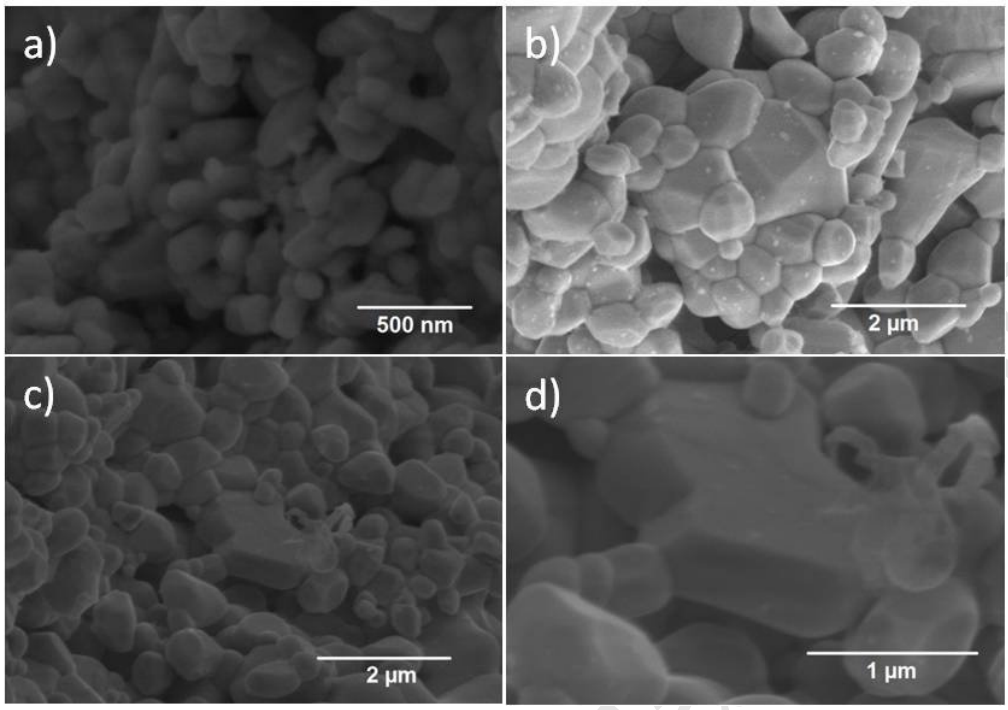

Figure 5: SEM images of a) HT_Bi3Mo1, b) HT_Bi2Mo3 and c-d) HT_Bi2Mo1 after catalytic propylene oxidation at temperatures up to 520 °C.

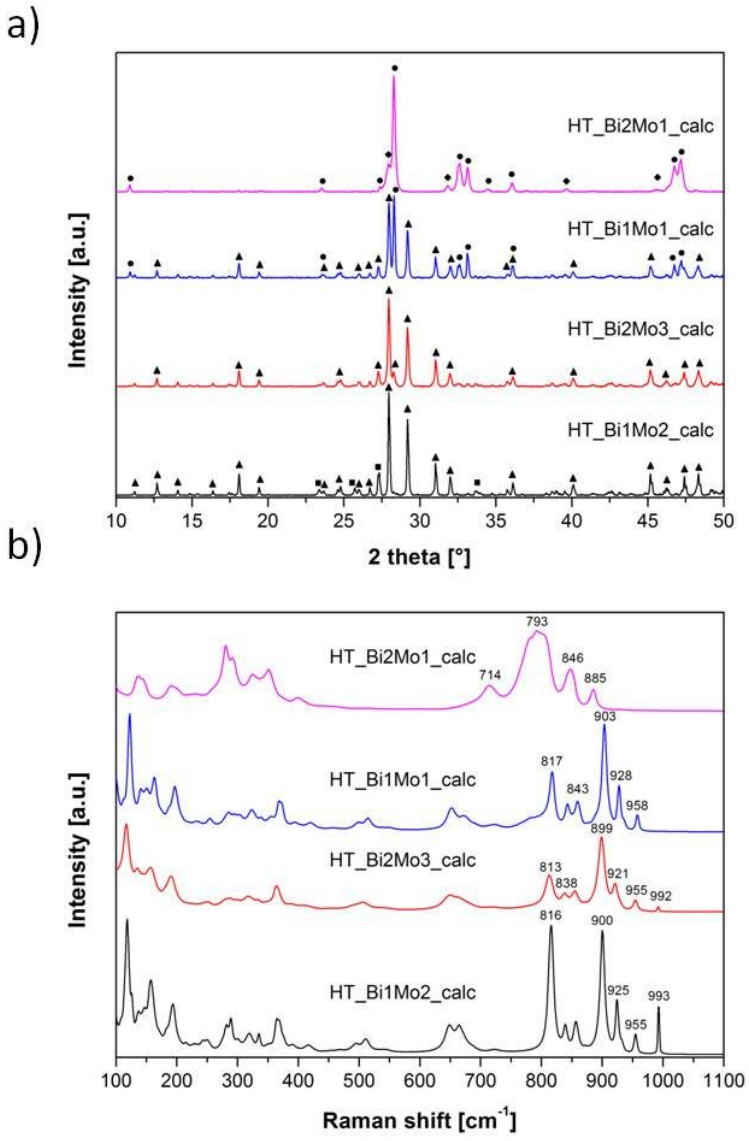

Figure 6: Characterization of the hydrothermally synthesized samples after calcination at 550 °C by X-ray diffraction (a) and Raman spectroscopy (b). γ-Bi_2MoO_6 (circles), β-$Bi_2Mo_2O_9$ (diamond), α-$Bi_2Mo_3O_{12}$ (triangle) and α-MoO_3 (993 cm^{-1}, squares).

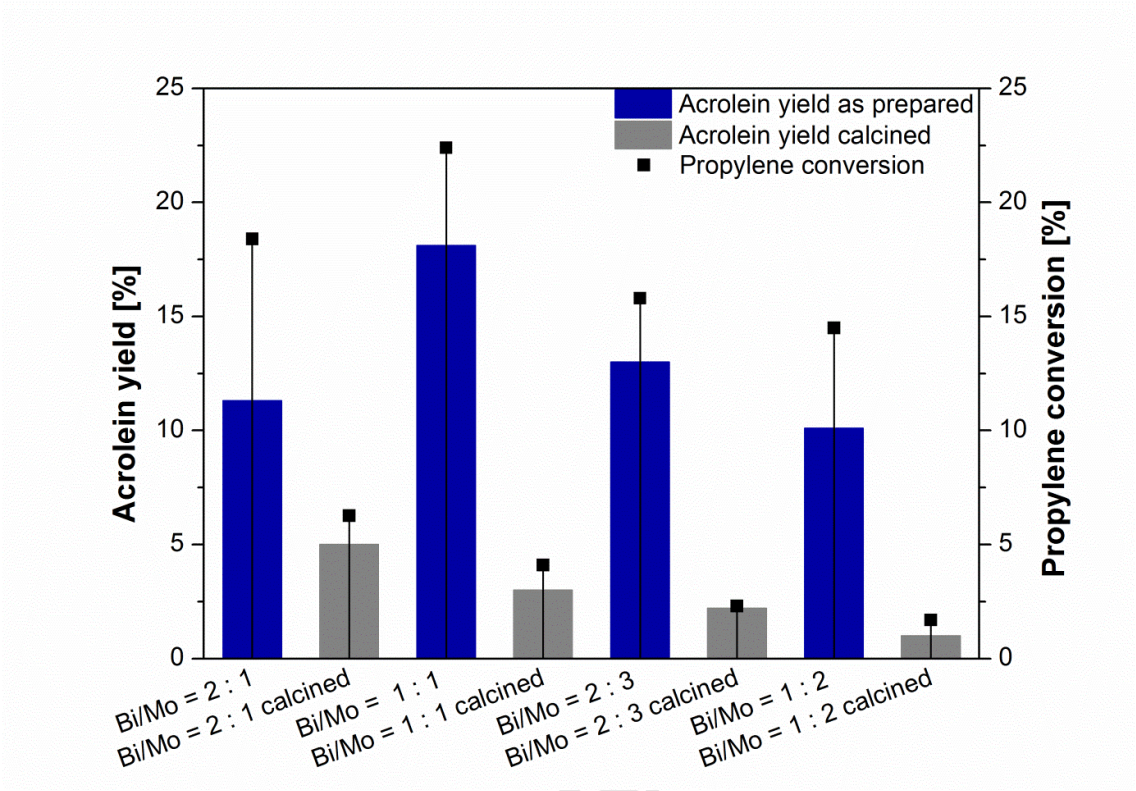

Figure 7: Catalytic performance of the hydrothermally synthesized samples with Bi/Mo ratios 2.0 – 0.5 at 480 °C with 120 Nml/min and a contact time of 0.11 (g·s)/ml (calculated at reaction temperature and pressure); black squares: propylene conversion, bars: acrolein yield (as prepared materials = blue, calcined samples = grey). For each sample the propylene conversion and the acrolein yield decreased after calcination.

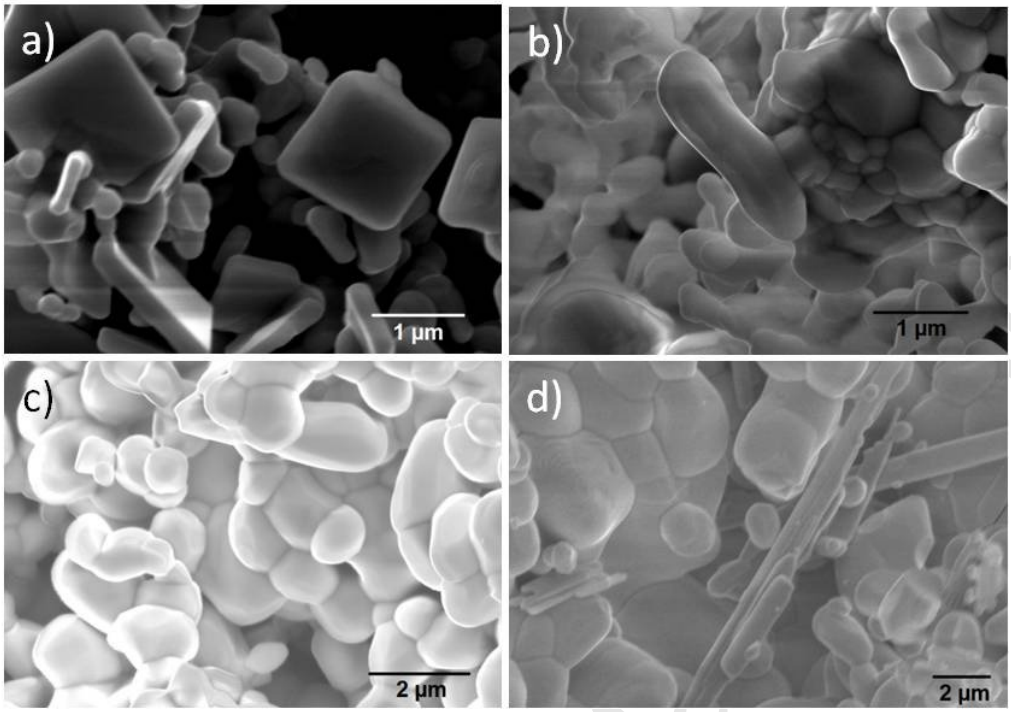

Figure 8: SEM images of samples synthesized with different Bi/Mo ratio after calcination at 550 °C a) HT_Bi2Mo1_calc, b) HT_Bi1Mo1_calc, c) HT_Bi2Mo3_calc and d) HT_Bi1Mo2_calc.

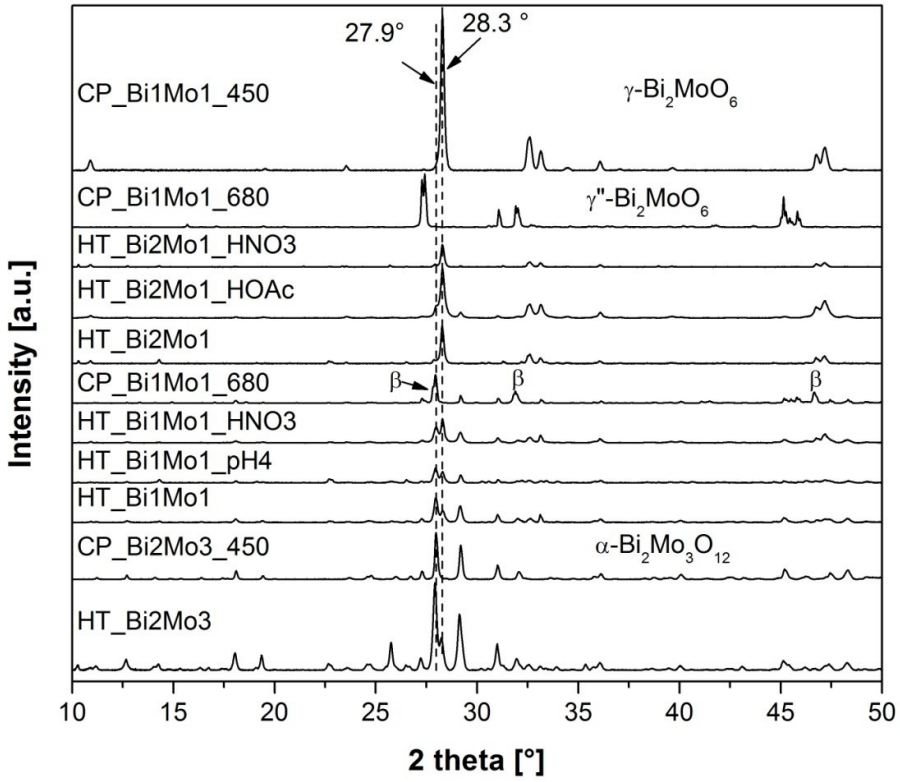

Figure 9: Powder X-ray diffraction pattern of the different samples prepared by co-precipitation (CP) and hydrothermal synthesis (HT) with Bi/Mo = 2:3, 1:1 and 2:1.

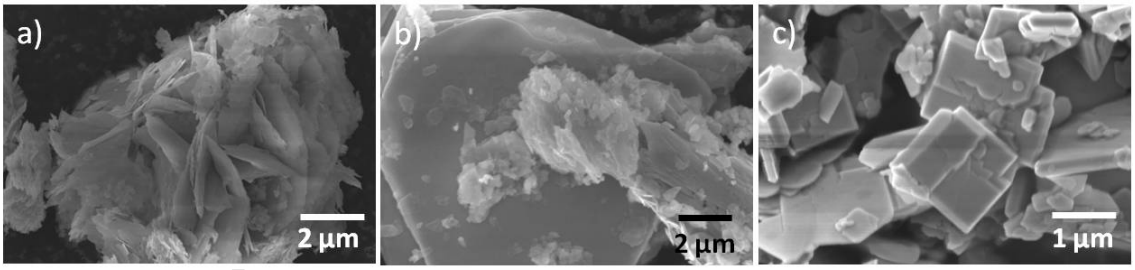

Figure 10: SEM images of a-b) HT_Bi2Mo1_HOAc and c) HT_Bi2Mo1_HNO3.

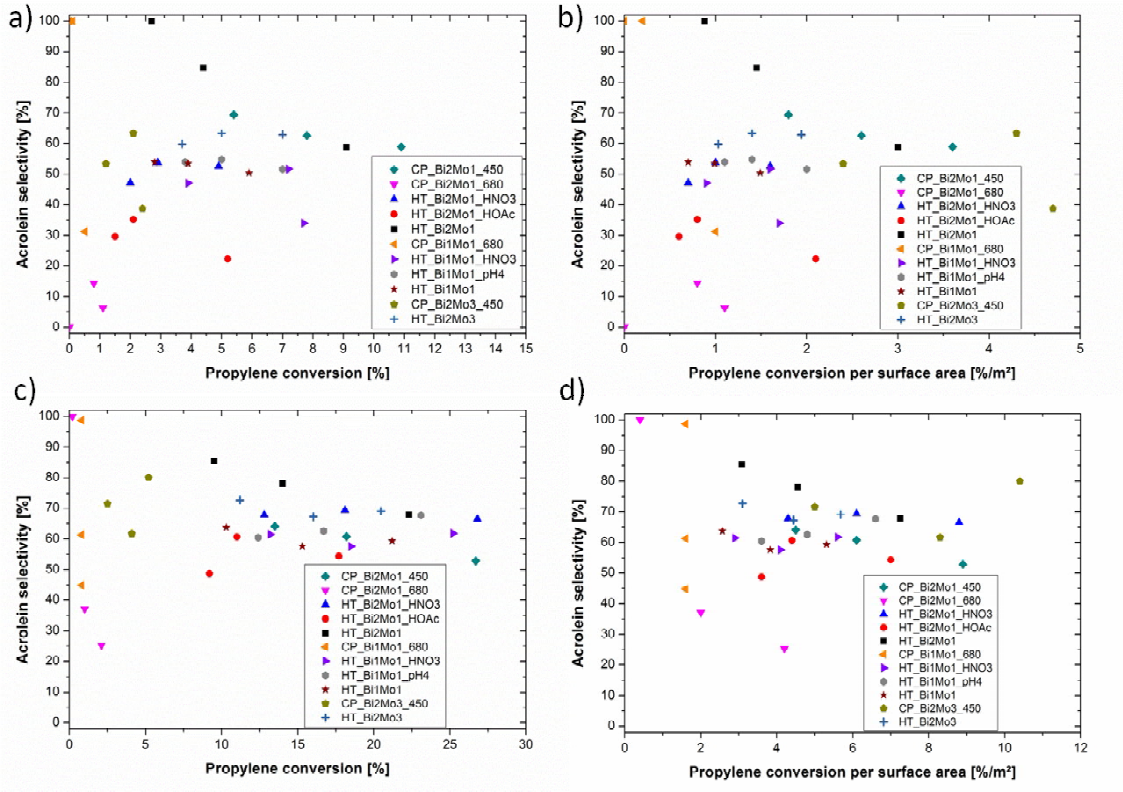

Figure 11: Catalytic performance of samples prepared by different methods with various Bi/Mo ratios at 320 °C (a, b) and 360 °C (c, d) with $C_3H_6/O_2/N_2$ = 5/25/70 applying total flows of 50, 80 and 120 Nml/min. Propylene conversion was also calculated on the basis of surface area (b, d) by dividing the conversion [%] by the surface area in the reactor [m²].

Highlights

- Bismuth molybdates with plate-like morphology were prepared by hydrothermal synthesis.
- Good catalytic activity and selectivity for propylene oxidation to acrolein.
- Thermal treatment decreased the propylene conversion resulting in lower acrolein yield.
- Addition of nitric acid or ammonia solution improved catalytic performance.
- Hydrothermal synthesis led to more active or selective catalysts than co-precipitation.

Graphical Abstract